ELSEVIER

Catalysis Today 77 (2002) 65–78

CATALYSIS TODAY

www.elsevier.com/locate/cattod

CO-free fuel processing for fuel cell applications

T.V. Choudhary, D.W. Goodman*

Chemistry Department, Texas A&M University, College Station, TX 77840, USA

Abstract

In view of the stringent CO intolerance of the state-of-the-art proton exchange membrane (PEM) fuel cells, it is desirable to explore CO-free fuel processing alternatives. In recent years, step-wise reforming of hydrocarbons has been proposed for production of CO-free hydrogen for fuel cell applications. The decomposition of hydrocarbons (first step of the step-wise reforming process) has been extensively investigated. Both steam and air have been employed for catalyst regeneration in the second step of the process. Since, PEM is poisoned by very low (ppm) levels of CO, it is essential to eliminate even trace amounts of CO from the reformate stream. Preferential oxidation of CO (PROX) is considered to be a promising method for trace CO clean up. Related studies along with a discussion of catalytic ammonia decomposition (for applications in alkaline fuel cells) will be included in this review.

Keywords: CO-free hydrogen; PROX; Fuel cells; Ammonia decomposition

1. Introduction

Fuel cell technology [1] offers highly efficient conversion of chemical energy into electrical energy without emission of environmental pollutants, thereby making fuel cells one of the most promising sources of power generation. The alkaline fuel cells (AFCs), the proton exchange membrane fuel cells (PEMs) and the phosphoric acid fuel cells (PAFCs), operate at low temperatures (<523 K), whereas the molten carbonate fuel cells (MCFCs) and solid oxide polymer fuel cells (SOFCs) operate at high temperatures (>923 K). The latter have a high tolerance for commonly encountered impurities such as CO and CO_2 (CO_x). However, the high temperatures required for these cells impose difficulties in their maintenance and operation making them unsuitable for vehicular and small-scale applications. Hence, a major part of the research (for small-scale applications) is currently being directed towards low temperature fuel cells. These low temperature fuel cells are extremely sensitive towards impurities such as CO_x; PAFCs can tolerate up to 2% CO, PEM only a few ppm whereas the tolerance level for CO_2 is extremely low (ppm level) in case of AFC.

Hydrogen is the most promising fuel for these fuel cells. Currently, steam reforming, partial oxidation and auto-thermal reforming of hydrocarbons are the major routes for hydrogen generation, but all these methods produce a large amount of CO_x as byproduct along with hydrogen [2–5]. Hydrogen generated by these conventional methods can be utilized by the low temperature fuel cells only if CO_x (CO for PEM and CO_2 for AFC) are completely eliminated from the stream prior to its introduction into the fuel cell. Fig. 1 shows the various processes involved when steam reforming of hydrocarbons is employed for hydrogen production. The products coming out of the steam reformer containing ca. 10% CO (depending on the feedstock and

* Corresponding author. Tel.: +1-979-845-0214; fax: +1-979-845-6822.
E-mail address: goodman@mail.chem.tamu.edu (D.W. Goodman).

0920-5861/02/$ – see front matter
PII: S0920-5861(02)00233-X

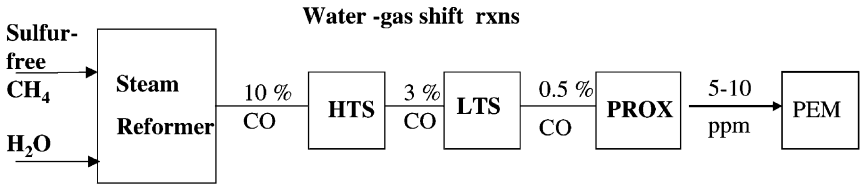

HTS: High Temperature Shift; LTS : Low Temperature Shift; PROX: Preferential Oxidation; PEM: Fuel

Fig. 1. Simplistic schematic of the methane steam reforming process for hydrogen generation for PEM fuel cells.

conditions employed) is passed into water gas shift reactors (WGSs) where CO is reacted with water to form CO_2 and hydrogen [6]. Generally two WGS reactors are used in series (high temperature and low temperature) to minimize the amount of water. The exit stream from the high temperature WGS reactor (operating temperature, 623–823 K; catalyst, iron oxide/chromium oxide) contains ca. 1.5–4% CO which is further reduced to 0.5–1% after the gases pass through the low temperature shift WGS reactor (operating temperature, 473–573 K; catalyst, $CuO/ZnO/Al_2O_3$). The WGS shift reactors are the bulkiest components of the fuel processing system. Finally, the CO content is reduced to a few ppm in the preferential oxidation reactor (PROX) [7]. The hydrogen can be introduced in the fuel cell only after this circuitous procedure of removing CO (AFCs would additionally require removal of CO_2 to ppm levels). Also, it is known that high levels of CO_2 in the hydrogen stream can be detrimental for the performance of PEM fuel cells. Other conventional process of hydrogen production such as partial oxidation and auto-thermal reforming also require similar procedures for CO_x removal. Removal of CO_x to ppm levels from the hydrogen stream makes the process extremely complex and bulky and thereby prohibits the use of the existing hydrogen production technology for use in vehicular and small-scale fuel cell applications. It is therefore of interest to explore other routes for hydrogen production with specific applications in fuel cells.

2. CO_x-free alternatives for hydrogen production

In the conventional hydrogen generation processes the hydrocarbons are converted to hydrogen in the presence of oxidants (air, oxygen or steam), thus resulting in the production of CO_x. As an alternative, if the hydrocarbons are reformed in a step-wise manner co-production of CO can be avoided [8,9]. This method involves the catalytic decomposition of hydrocarbons [10,11] in the first step (should be theoretically CO_x-free) following which the catalyst is regenerated (with steam/air) in another step. This two step process when operated in cycles represents a potential CO_x-free route for hydrogen production (in Step I of the process) for fuel cell applications.

The other approach involves the use of a feedstock that is not carbon based. The catalytic decomposition of ammonia appears to be an appealing process for clean hydrogen production [12,13]. Ammonia decomposition for production of mass-scale hydrogen for general purposes would be self-defeating as ammonia itself is produced from hydrogen, but appears to be promising from the view of specific fuel cell applications. Transportation and storage of hydrogen is a complex issue. Ammonia on the other hand can be stored/transported as a liquid at room temperature and 8 bar pressure. This mildly endothermic process involves the cracking of ammonia into hydrogen and nitrogen.

$$2NH_3 \rightarrow N_2 + 3H_2 \qquad \Delta H = +11\,\text{kcal/mole}$$

The process operated in this way produces no CO or CO_2 [14,15] forming nitrogen as the only co-product (essentially benign to the fuel cell). Steam reforming of methanol is often touted as a hydrogen source for acid fuel cells. However, a comparison of economics for hydrogen production via ammonia decomposition for an AFC as opposed to hydrogen production via steam methanol reforming for acid fuel cells, suggests that ammonia is a better choice [12,13]. Bulk ammonia

is prepared at 99.5% impurity (impurity is mainly water: harmless to the fuel cell) [1]. In contrast, the higher alcohol impurities present in commercial methanol can result in production of contaminants during reforming that can lead to poisoning of the fuel cell electrodes. With these considerations, catalytic decomposition of ammonia appears to be an interesting route for production of hydrogen for AFC. Ammonia can also be used as a source of hydrogen for acid fuel cells if the unreacted ammonia in the hydrogen stream is scrubbed prior to introduction in the fuel cell.

In this work, we intend to review studies related to hydrocarbon decomposition, step-wise hydrocarbon reforming, preferential CO oxidation and ammonia dehydrogenation.

3. Catalytic decomposition of hydrocarbons

This section focuses on the first step (catalytic decomposition) of the step-wise reforming process. The large abundance of methane (in form of natural gas) and its high H/C ratio makes it an ideal hydrocarbon feedstock for the proposed process. Decomposition of methane has been studied quite extensively for methane homologation reactions [16–19] and fundamental dynamic studies [20–22]; however methane decomposition as a method to obtain hydrogen for fuel cell applications has received relatively less attention. This is rather surprising, as first order mass and energy balance comparison for various hydrogen production processes have shown methane decomposition to require the least amount of process energy for hydrogen production [23].

Muradov has investigated methane decomposition over a large number of carbon-based catalysts [24]. Amongst the various catalysts tested for the thermo-catalytic methane cracking, activated carbon from coconut shells showed the highest initial activity whereas graphite showed the least. The difference in activity of the catalysts was related to the structure and size of carbon crystallites; similarity with graphitic type structure resulted in low methane decomposition activity. The study involving methane decomposition in binary mixtures with different hydrocarbons over inert supports yielded interesting results; while addition of acetylene was found to enhance the methane decomposition activity, addition of propane was not beneficial. The increase in hydrogen yield on acetylene addition was attributed to the catalytic effect of carbon formed from acetylene decomposition; significantly smaller sizes of the carbon crystallites were formed from acetylene (5 nm) as compared to that from methane (80 nm).

Previously, it has been noted that methane decomposition may lead to CO formation via reaction of the carbonaceous residue with the oxygen of the oxide support [25]. The main objective of the methane decomposition studies by our group was to address crucial issues such as the role played by the support in determining the CO content and nature of surface carbon [10,26]. The CO formation rates showed a common trend for all the catalysts; high initial rates that rapidly decreased with time and finally stabilized [26]. The CO content in the hydrogen stream was ca. 50, 100 and 250 ppm for Ni/SiO_2, $Ni/SiO_2/Al_2O_3$ and Ni/HY, respectively, after the CO formation rates had stabilized. This support dependence on the CO formation rate was related to the difference in the amount/stability of the –OH groups present on the different supports. Fig. 2 shows the time on stream hydrogen formation activity and CO content on the Ni/SiO_2 catalyst at 823 K. The rate of CO formation was found to increase with increasing temperatures and decrease with increasing gas space velocities (decrease in contact time) [26]. The space velocity effect was especially dominant in the initial period of the methane decomposition reaction (Fig. 3).

Time on stream methane activity studies for the various Ni-supported catalysts at 823 K [26] showed comparable initial methane decomposition activities (with the exception of 10% Ni/activated carbon, in which case it was much lower) but widely different catalyst stabilities. While rapid deactivation (in ca. 1 h) was observed in case of HZSM-5 and carbon support the stability of the Ni/SiO_2, Ni/HY and $Ni/SiO_2/Al_2O_3$ catalysts for methane conversion was much higher (several hours). TEM images of Ni/HZSM-5 catalyst after the reaction showed an encapsulating type of carbon, which explained the rapid deactivation of the catalyst. On the other hand, filamentous carbon formation was observed in case of Ni/SiO_2, Ni/HY and $Ni/SiO_2/Al_2O_3$ catalysts [10]. In case of filamentous carbon, the Ni particle (active component) is present at the apex of the particles resulting in a larger life-time of the catalyst (Fig. 4). In fact carbon amounts greater

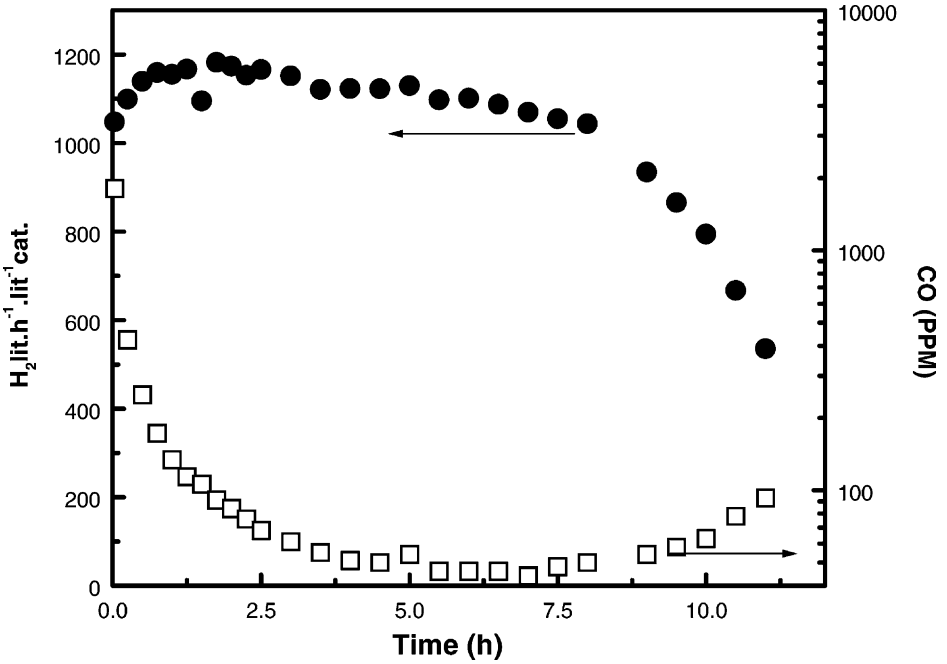

Fig. 2. Hydrogen formation rate and CO content (in H_2) during methane (20% CH_4 in Ar) decomposition on Ni/SiO_2 at 823 K; GHSV = 20,000 cc/g/h [10].

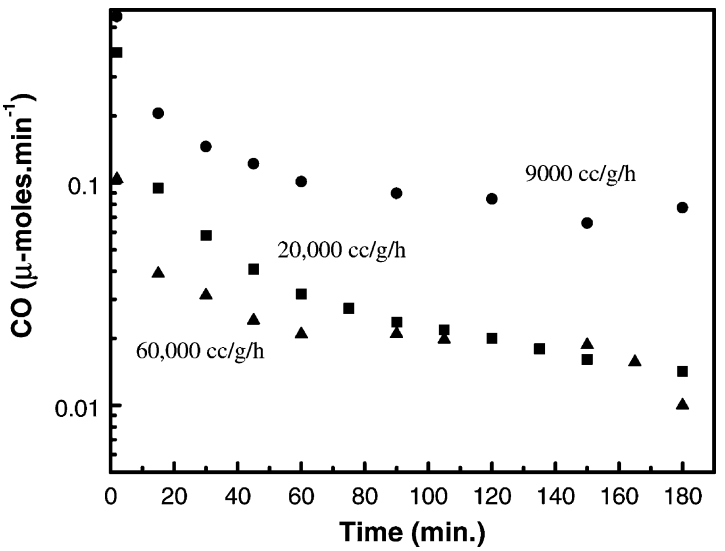

Fig. 3. Effect of space velocity on the CO formation rate during methane decomposition on Ni/SiO_2 at 823 K (feed: 20% CH_4 in Ar) [26].

Fig. 4. TEM image of a single filament of carbon.

than 200 $g_C/g_{catalyst}$ can be obtained under optimum conditions of filament formation [27,28]. In the past, Baker and co-workers have extensively investigated filamentous carbon formation from a variety of hydrocarbons [29–31]; an excellent review on filamentous carbon can be found in [32]. There is currently a great interest in these carbon nano-tubes [33–35], as the unique properties exhibited by these materials can be exploited in a number of applications (catalyst support, energy storage devices, selective adsorption agents and reinforcement materials [36–39]).

Recently, Otsuka et al. [40] have observed greater than equilibrium methane (decomposition) conversion on Ni/SiO_2 in presence of $CaNi_5$ (physical addition). This effect was attributed to the hydrogen absorption property of $CaNi_5$, which assisted in shifting the reaction equilibrium to the right hand side. The same group [41] subsequently investigated the nature of the surface carbon formed after decomposition of different hydrocarbons (CH_4, C_2H_6, C_2H_4, C_2H_2, C_3H_8 and C_3H_6) on Ni/SiO_2. While zigzag fibers (carbon nano-tubes) were obtained from methane decomposition, alkene and acetylene decomposition produced rolled fiber structures. Raman spectroscopy studies further revealed that the degree of graphitization was also dependent on the nature of the hydrocarbon employed. The catalytic life of the Ni/SiO_2 catalyst for the decomposition reaction decreased in the order: alkanes > alkenes $\gg$ acetylene.

The use of solar power as a clean source of process energy is an interesting approach for controlling CO_2 emissions. Steinfeld et al. [42,43] performed methane/butane decomposition experiments on Co and Ni-supported catalysts in a fluidized bed reactor at the

PSI solar furnace (consisting of a sun-tracking heliostat and stationary concentric parabolic dish); vigorous bubbling conditions were maintained in the fluidized bed to operate at uniform temperatures. Concomitant with the gaseous hydrogen product, carbon filaments were formed on the surface of the catalysts. High resolution transmission electron microscopy (HRTEM) studies showed no significant differences between the carbon filaments formed from methane and butane.

Application of membrane reactors for hydrocarbon reforming can effectively increase the yields of hydrogen [44]. Ishihara et al. observed greater than equilibrium methane conversions using a 90% Pd–10% Ag hydrogen permeable membrane reactor during the decomposition of methane over Ni/SiO_2 catalyst [45]. The permeated hydrogen was swept by argon gas; increase in Ar flow-rates resulted in enhanced methane conversion. Since the hydrogen permeability increased with increasing temperature, the positive effects in the hydrogen yields were more pronounced at higher temperatures (>700 K). A constant conversion of 70% (10% CH_4 in N_2) was observed at 773 K over a time period of 60 h. A membrane type of reactor has recently been employed to study ethane and gasoline decomposition on a Ni/Ca/carbon catalyst [46]. The membrane reactor decreased methane formation during ethane cracking (as opposed to a fixed bed reactor), and thereby increased the hydrogen yield. Similarly the membrane reactor also enhanced the hydrogen yields from gasoline decomposition.

4. Step-wise reforming of hydrocarbons

The step-wise reforming of hydrocarbons has been employed in the past by Universal oil products (Hypro process) [47]. The process utilized a 7% Ni/Al_2O_3 catalyst in a fluidized bed reactor regenerator. Catalytic decomposition of methane occurred in the fluidized bed reactor at ca. 1150 K following which the deactivated catalyst was continually transferred into the fluidized bed regenerator. The carbon deposited in the catalytic decomposition step was removed in the fluidized bed regenerator by air at ca. 1475 K and then transported back to the fluidized bed reactor. The process operated in this manner resulted in a product stream containing 93–95% hydrogen; the remainder being mostly unreacted methane. Though this process is much simpler than the steam reforming process, the steam reforming process has an economic advantage when employed for extremely large-scale production of hydrogen (as large fluidized beds and solid circulation systems are very expensive). However, the process is extremely suitable for application in small installations, e.g. hydrogen production for fuel cell applications.

We have recently investigated the step-wise steam reforming process in our laboratory [8,9]. The process can be represented as:

$$CH_4 \rightarrow \frac{C_{ads}}{[C(H)_n]_{ads}} + \left(2 - \frac{n}{2}\right) H_2 \qquad \text{Step I}$$

$$\frac{C_{ads}}{[C(H)_n]_{ads}} + 2H_2O \rightarrow CO_2 + \left(2 + \frac{n}{2}\right) H_2 \qquad \text{Step II}$$

The studies were performed in a pulse mode so as to ensure accurate quantitative analysis of the carbon removed in the regeneration step. Table 1 shows the data for 16 reaction cycles (Step I + Step II) on 200 mg 88% Ni/Zirconia at 648 K. No catalyst deactivation was observed in this study; in contrast consequent pulsing of methane without intermittent regeneration (i.e. without Step II) showed an exponential deactivation of the catalyst. The amount of surface

Table 1
Sixteen reaction cycles on Ni/Zirconia at 648 K showing the amount of methane reacted in Step I (methane decomposition) and carbon containing products formed in Step II (steam gasification)

Cycle	CH_4 reacted in Step I[a]	Step II[a]	
		CO_2 formed	CH_4 formed
1	3.4	1.8	1.6
2	3.4	2.6	0.7
3	3.4	2.4	0.8
4	3.4	2.6	0.6
5	3.4	2.5	0.6
6	3.4	2.6	0.7
7	3.4	2.6	0.7
8	3.4	2.5	0.7
9	3.4	2.5	0.7
10	3.4	2.4	0.8
11	3.4	2.3	0.8
12	3.4	2.5	0.8
13	3.4	2.3	0.8
14	3.4	2.5	0.7
15	3.4	2.6	0.8
16	3.4	2.6	0.7

[a] All units in (μmoles).

carbon removed varied from 92 to 100% (of the amount deposited in Step I) in the various cycles; 95% of the carbon was removed on an average. It should be noted that no filamentous carbon was observed on the surface in these pulse experiments. The CO content in the hydrogen produced in Step I was less than 20 ppm. The average amount of hydrogen produced per mole of methane consumed in Step I was 1.1, thus suggesting the presence of residual hydrocarbonaceous species on the catalyst surface. Our recent neutron vibrational spectroscopy studies have revealed the presence of methylidyne (CH), vinylidene (CCH_2) and ethylidyne (CCH_3) species on Ni-based surfaces after methane dissociation at low temperatures (<673 K) [48]. The ethylidyne species were less stable than the vinylidene and methylidyne species with increasing methane decomposition temperatures.

Amiridis and co-workers employed a continuos flow reactor [49] to study the step-wise steam reforming process. In the first step, methane was decomposed over 15% Ni/SiO_2 catalyst at 923 K and gas hourly space velocity of 30,000 h^{-1} for 3 h. In the second step, the catalyst was regenerated with steam until no hydrogen was observed in the product stream. Ten reaction cycles performed as described above showed no significant decrease in catalytic activity [49]. X-ray diffraction (XRD) patterns collected after individual cycles suggested that a large amount of the carbon deposited in Step I was removed in the regeneration step. Also the XRD pattern after the 10th cycle was found to be similar to that after the first cycle indicating the absence of carbon accumulation with increasing number of cycles. It is noteworthy that there was no significant change in the crystallite size of Ni during the reaction–regeneration cycles. Our recent studies on a pulse mass analyzer balance show that ca. 75% of the surface carbon (deposited in Step I on $Ni/Al_2O_3/SiO_2$ at 823 K) can be removed during the steam regeneration step (823 K) in the continuos flow mode [26].

Choudhary et al. have investigated the step-wise steam reforming process in two parallel reactors [50]; methane decomposition and gasification were carried out simultaneously by switching a methane containing feed and steam containing feed between the two reactors at pre-determined time intervals. Amongst the various Ni-supported catalysts (ZrO_2, MgO, ThO_2, CeO_2, UO_3, B_2O_3, MoO_3, HZSM-5, Hβ, NaY, Ce(72)NaY and Si-MCM-41) tested for this cyclic reaction, Ni/ZrO_2 and Ni/Ce(72)NaY were found to be the most suitable catalysts. Carbon balance after 36 reaction cycles on Ni/ZrO_2 at 773 K showed that major part of the deposited carbon could be removed. The main advantage of this cyclic process was the absence of a pressure drop across the catalyst bed during the process, which would be observed if the reaction had been carried out without intermittent regeneration cycles. It is noteworthy that the performance of the catalyst was dependent on the feed switch over time.

In line with the Hypro process, air can be used instead of steam in the regeneration step. Utilization of air can effectively increase the energy efficiency of the process as the exothermic regeneration step can be employed to drive the endothermic hydrocarbon decomposition step. However on the negative side, air regeneration may lead to sintering of the catalyst. We have recently investigated the reaction/regeneration (by air) cycles on 10% Ni/HZSM-5 at 723 K [10] in a fixed bed reactor. In this case, the methane decomposition step was performed for 1 h following which the catalyst was regenerated using an oxidation–reduction cycle. There was no apparent decrease in catalytic activity throughout the 12 cycles studied at 723 K. Similarly, Monnerat et al. [51] have investigated the cyclic process (methane decomposition and air regeneration) over a Ni gauze catalyst (Ni-grid with Raney type outer layer). Their studies revealed an optimal reaction performance when the cycle consisted of 4 min of reaction period followed by 4 min of regeneration period. Surprisingly the authors observed a lack of dependence of the CO_x (CO or CO_2) selectivity on the cycle duration. In a second study, Mirodatos and co-workers [52] investigated the same process on a Pt/CeO_2 catalyst at 673 K under forced unsteady-state conditions. No CO was detected in the products under these conditions in either the cracking or the oxidative regeneration steps.

Otsuka et al. have employed a process which involves a metal oxide-mediated storage of hydrogen formed from methane cracking [53,54]. The method consists of the following steps: (1) hydrogen production via methane decomposition in the first step; (2) reduction of metal oxides by hydrogen; and finally (3) release of the stored hydrogen by contact with water vapor at 673 K (when CO-free hydrogen is required). While Ni/SiO_2 was utilized for the cracking

of methane [55], iron oxide and indium-based oxides were employed for hydrogen storage [53].

5. Preferential oxidation of CO (PROX)

PROX is one of the most effective methods for trace CO clean up from the reformate stream prior to its introduction in the PEM cell. In this section, a brief overview of the studies related to this system is provided. High CO oxidation activities coupled with low hydrogen oxidation activities (at the desired operating temperature) are essential requirements for PROX catalysts.

The PROX reaction has been extensively investigated on Pt/Al_2O_3 catalysts [56–61]. Oh and Sinketvitch [59] observed a maximum in CO conversion with temperature on 0.5% Pt/Al_2O_3 at ca. 473 K in the presence of excess hydrogen in the feed stream. In contrast, a constant conversion of 100% (above ca. 473 K) was observed in absence of hydrogen. A similar trend has been observed by Kahlich et al. [60] on a 0.5% Pt/γ-Al_2O_3 catalyst. The decrease in CO conversion (in presence of hydrogen) with increasing temperature was attributed to a greater contribution from the competitive H_2 oxidation at higher reaction temperatures. It is noteworthy that the presence of hydrogen caused a decrease in the ignition temperature for the CO oxidation reaction [59,60]. The Pt/Al_2O_3 catalyst showed no significant CO methanation activity in the temperature range between 423 and 523 K [60]. The kinetic studies for the PROX reaction showed reaction orders of -0.4 and $+0.8$ with respect to CO and O_2, respectively, and an apparent activation energy of 17 kcal/mol. Along with the adsorbed CO species, formate species were observed on the surface during the PROX reaction (in situ DRIFTS) [61]. Presence of hydroxyl groups (of the support) was found to be essential for the formation of the surface formates.

Watanabe and co-workers investigated the PROX reaction on zeolite-supported Pt catalysts [62,63]. Preliminary studies [62] on Pt/A-zeolite catalyst showed extremely promising results; an order of magnitude higher CO oxidation selectivity (as compared to Pt/Al_2O_3) was obtained at similar conversion levels. Subsequent studies [63] involving a series of catalysts (Pt/A, Pt/modernite, Pt/X, Pt/Al_2O_3) showed that the Pt/modernite catalyst required the least amount of excess oxygen for the complete conversion of CO (1%) in presence of excess of hydrogen. Use of a two-stage reactor further increased the effectiveness of the Pt/modernite catalyst. Also, the catalyst performance was not significantly influenced by the presence of water in the feed stream.

Oh and Sinketvitch [59] compared the efficiency of several noble metals for the PROX reaction; the CO conversion was found to decrease in the following order: $Ru/Al_2O_3 > Rh/Al_2O_3 > Pt/Al_2O_3 > Pd/Al_2O_3$ (metal loading 0.5 wt.% for all catalysts). While Pd showed a similar CO oxidation activity to Ru and Rh at lower temperatures, it showed significantly inferior activity at higher temperatures. This effect was attributed to the change in oxidation state (highly active reduced form to less active oxidized form) of Pd with increasing reaction temperature. Although this study clearly shows the high efficacy of Ru and Rh, these catalysts, surprisingly, have not been explored subsequently in greater details.

In recent years, there has been great interest in investigating the CO oxidation reaction over gold-based catalysts [64–71]. Although bulk gold is highly inefficient for CO oxidation, supported nano-gold clusters have incredible CO oxidation activity; these catalysts show high activity even at sub-ambient temperatures. The nano-gold catalysts are also extremely promising from the point of view of the PROX reaction; while bulk gold and larger Au particles show higher oxidation activity for H_2 as compared to CO, the situation is entirely reversed for supported nano-gold catalysts (Table 2). Haruta and co-workers observed a greater than 95% conversion for CO (1% CO, 1% O_2, balance H_2) in a temperature range between 323 and 353 K [72]. This clearly is very promising, as the normal operation temperature of a PEM cell is ca.

Table 2
Comparison of activities for CO and H_2 oxidation (in terms of temperature required for 50% conversion) on Au-based catalysts

Catalyst	$\langle d_{Au} \rangle$ (nm)	$T_{1/2}$ CO (K)	$T_{1/2}$ H_2 (K)	Reference
Au powder	20	573	373	[64]
2% Au/TiO_2	1.7	237	313	[65]
6.6% Au/SiO_2	6.6	227	329	[65]
14.7% Au/SiO_2	20	668	589	[65]
0.94% Au/Al_2O_3	2.4	290	362	[65]
5% Au/Al_2O_3	23	503	433	[68]

353 K. Alumina-supported nano-gold catalysts have also been effectively employed as PROX catalysts [73]. The conversion and selectivity for CO oxidation was further enhanced by addition of MgO and MnO_x to the Au/Al_2O_3 catalysts [74]. The promoted catalysts showed selectivities greater than 90% for the PROX reaction at temperatures $\leq$373 K.

Catalyst comparison studies by Kahlich et al. for the Au/Fe_2O_3 [75] and Pt/Al_2O_3 [60] systems for the PROX reaction has revealed the former to be a better catalyst for the following reasons: (1) higher CO oxidation activity at lower temperature (353 K) and (2) lower hydrogen consumption. However, Pt catalysts have an advantage over Au catalysts in terms of stability. In general, nano-Au catalysts are known to undergo rapid deactivation during CO oxidation [70,76–78]. Extensive efforts have been undertaken in our laboratory to study the deactivation mechanism [65,76–81]; STM/STS studies on model Au catalyst studies have shown that the deactivation is induced by oxygen.

In order to employ Au as PROX catalysts, it is essential to synthesize nano-Au catalysts with high stability towards CO oxidation. Recently, we obtained highly active and fairly stable catalysts by a temperature programmed reduction–oxidation treatment of an Au–phosphine complex on TiO_2 [82]. Time on stream CO oxidation studies revealed a slow initial deactivation followed by stable activity for several hours (Fig. 5). Moreover, the catalyst could be completely regenerated by a reduction–oxidation treatment. Longer time on stream studies under varying experimental condition are currently underway.

Other systems, which have been investigated for the PROX reaction include metal oxides [83] and bimetallic [84] catalysts. PROX studies over catalysts consisting of 3d transition metal oxides have revealed CoO to be an interesting candidate for the desired reaction [83]. It showed a near 100% CO conversion (feed: 1% CO; 1.86% O_2; 90% H_2 and balance N_2) and selectivity of ca. 60% for CO_2 formation at 403 K; the catalyst activity was maintained for >20 h in this study. NiO and CuO were found to catalyze the CO methanation reactions at temperatures above 473 and 573 K, respectively, these temperatures corresponded to the reductive transformation of the metal oxide catalysts.

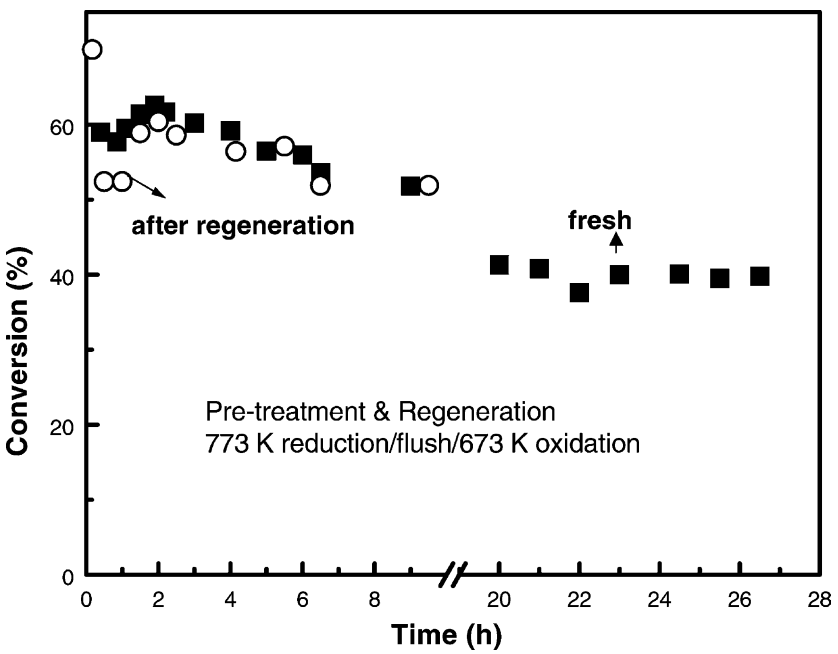

Fig. 5. Catalyst stability/regeneration after CO oxidation on Au/TiO_2 at 313 K (GHSV = 20,000 cc/g/h; P_{CO} = 27.5 Torr and P_{O_2} = 55 Torr) [82].

Schubert et al. [84] have recently reported a superior CO oxidation activity and selectivity (than Pt/Al_2O_3) for a bimetallic carbon-supported PtSn system at low temperatures (273–353 K). Unlike in case of Pt/Al_2O_3, the CO oxidation reaction was not limited by CO desorption for the carbon-supported PtSn catalysts. Based on their spectroscopic studies the authors proposed a mechanistic model involving competitive adsorption of CO and H_2 on Pt sites, and O_2 adsorption mainly on Sn sites and SnO_x islands present in the vicinity of the active PtSn particles.

6. Catalytic decomposition of ammonia

Ammonia decomposition on metal surfaces has been extensively studied for enhancing the understanding of the industrially important ammonia synthesis process [85–90]. However, only a few of these investigations provide information related to the topic of interest of this review, i.e. hydrogen production.

Recently, Papapolymerou and Bontozoglou have compared the ammonia decomposition activity for various metal wires [91]. Their investigation showed that Ir wires were far more active than Pd, Pt and Rh. Also comparison with previous studies show higher ammonia decomposition rates on Ir [91,92] as opposed to Ni wires [93]. This motivated us to investigate the ammonia decomposition process on Ir single crystal surfaces [15]. In these studies the ammonia decomposition experiments were performed in the elevated pressure reactor whereas the pre- and post-reaction surface analysis was accomplished in a contiguous UHV chamber by Auger electron spectroscopy (AES). The kinetics of the reaction was measured by following the total pressure (in the static reactor) during the course of the reaction. Fig. 6 shows the decomposition of ammonia with initial pressure

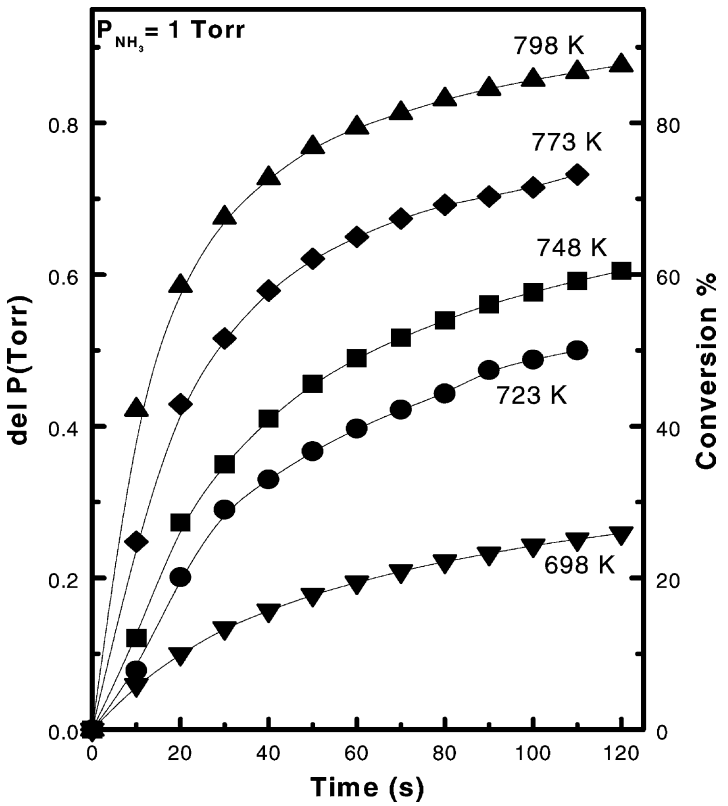

Fig. 6. Total pressure change (ammonia conversion) during ammonia decomposition on Ir(1 0 0) as a function of reaction time [initial $P(NH_3) = 1$ Torr] [15].

of 1 Torr at different reaction temperatures. The ammonia conversions increased linearly with time for the first few seconds following which there was a slow gradual increase. A similar trend was also observed in other cases where, initial partial pressures of ammonia were varied. The activation energy (ca. 20 kcal/mole) obtained in this study was in excellent concurrence with the value obtained on the supported Ir catalysts. For comparison, the activation energy values obtained for ammonia decomposition on various metal surfaces are shown in Table 3. Temperature programmed desorption (TPD) studies revealed that the activation energy for the recombinative nitrogen desorption (15.3 kcal/mole) was comparable to the apparent ammonia decomposition activation energy, suggesting that the nitrogen desorption was the rate limiting step for the process [94].

The reaction orders for the ammonia decomposition (from previous literature [95,96]) reaction vary from 0.5 to 1.35 for ammonia and −0.6 to −2.45 for hydrogen depending on the metal investigated. Our kinetic studies revealed reaction orders of 0.9 and −0.7 for ammonia and hydrogen, respectively, on Ir(1 0 0). TPD experiments were performed to understand the negative order of hydrogen. Fig. 7 shows the TPD spectra for the $^{15}ND_3$ covered Ir(1 0 0) surface with and without co-adsorbed hydrogen. The co-adsorption of hydrogen was found to increase the desorption temperature for HD, $^{15}ND_3$ and N_2, indicating the enhancement of the rate of the reverse reaction ($NH_x + H \rightarrow NH_{x+1}$; $x = 0$–2) in the presence

Table 3
Activation energies for the ammonia decomposition reaction on various surfaces

Catalyst	Temperature range (K)	E_a (kcal/mole)	Reference
Ru film	543–738	45	[95]
Ru(0 0 1)	<650	43	[96]
Ru/Al_2O_3	623–723	21	[97]
Ru/C	623–723	23	[97]
Ru-CeO_2/YZ	573–623	16	[98]
Ru/SiO_2	573–723	20	[14]
Ru/Al_2O_3	573–723	19	[14]
Ni film	663–773	43	[95]
Ni wires	<1000	50	[93]
Ni/HY	573–773	20	[14]
$Ni/SiO_2/Al_2O_3$	573–773	22	[14]
Ni/SiO_2	573–773	21	[14]
Pt film	793–883	59	[95]
Rh film	693–773	57	[95]
Fe film	605–743	39	[95]
Ir wires	900–2000 K	19	[92]
Ir wires	<750 K	31	[91]
Ir(1 0 0)	698–798	20	[15]
Ir/Al_2O_3	573–723	20	[14]
Ir/SiO_2	573–723	17	[14]

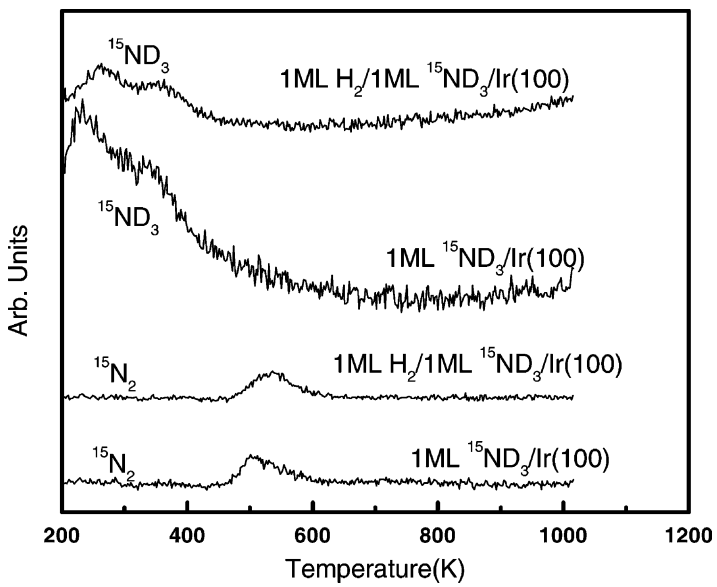

Fig. 7. Comparison of the $^{15}ND_3$ TPD spectra on Ir(1 0 0) surfaces obtained in the presence and absence of 1 ml H_2 [15].

Table 4
Conversion of ammonia and hydrogen formation rates for silica containing catalysts

Temperature (K)	10% Ni/SiO_2		10% Ir/SiO_2		10% Ru/SiO_2	
	Conversion (%)	Rate (H_2) mmol/min/$g_{catalyst}$	Conversion (%)	Rate (H_2) mmol/min/$g_{catalyst}$	Conversion (%)	Rate (H_2) mmol/min/$g_{catalyst}$
673	1.4	0.44	3.9	1.2	14.3	4.5
723	4.2	1.3	8.1	2.6	36.4	11.4
773	10.5	3.3	18.2	5.7	64.0	20.0
823	21.6	6.8	30.4	9.5	–	–
873	36.4	11.4	56.0	17.6	97	30.3
923	70.0	21.1	–	–	99	30.9
973	–	–	98	30.6	–	–

of excess hydrogen. Essentially, the (forward) ammonia decomposition reaction occurred at higher temperatures in the presence of excess hydrogen atoms.

Concomitant with the model catalyst studies we also investigated the decomposition of ammonia on various metal-supported catalysts [14]. The activation energies (E_a) for the ammonia decomposition processes varied from 17 to 22 kcal/mole depending on the catalyst employed. As seen from Table 3, the E_a values obtained in this study for Ru catalysts are in good agreement with those obtained by Bradford et al. [97]. The E_a values for Ni [14] and Ru-supported [14,97] catalysts were found to be lower than reported values on pure metal catalysts (films/wires/single crystal) [93,95], whereas Ir-supported catalysts [14] were in excellent agreement with Ir metal [15,92]. This suggests that the metal support interaction plays an important role in determining the apparent E_a of the catalyst.

Ammonia decomposition activity per site was found to increase in the order Ni < Ir < Ru [14]. The ammonia conversion (disregarding metallic dispersion) also showed the same trend (Table 4). Conversions approaching 100% were obtained at 900 and 973 K for Ru/SiO_2 and Ir/SiO_2, respectively. Hydrogen production activity for Ni-supported catalysts though lower was not significantly different making it suitable from an economic standpoint. Interestingly, the supports were found to strongly influence the hydrogen formation rates. Although, Ni/HZSM-5 had the highest dispersion amongst the Ni-based catalysts, it showed the least conversion. In the case of the Ru and Ir catalysts, the ammonia decomposition activity per site was found to be greater on silica as opposed to alumina. This profound influence of the support for the catalytic decomposition of methane has also been observed by Vannice and co-workers; 1.6% Ru/Al_2O_3 was found to have an order of magnitude greater ammonia decomposition activity per site than 4.8% Ru/C [97]. In a recent study, a Ru-CeO_2 catalyst supported on Y-form zeolite was found to be highly active for ammonia decomposition [98]. The reaction was found to be first order with respect to ammonia with an E_a of 16 kcal/mol. As in previous studies, desorption of nitrogen was determined to be the rate limiting step for the decomposition reaction [86,95].

Thermodynamic calculations on ammonia cracking show that an equilibrium conversion of 97% can be obtained at 10 bar pressure and 723 K. It is therefore of considerable interest to develop catalysts, which can approach these high conversions at low temperatures. Recently, it has been shown that addition of potassium results in a tremendous increase in the rate of ammonia decomposition [99,100]. Thus, it is of utmost importance to thoroughly investigate the role of the promoters and supports, etc. in the catalytic ammonia decomposition process to meet the desired objectives.

7. Concluding remarks

Fuel processing represents a very important aspect of fuel cell technology. The widespread utilization of fuel cells will only be possible if CO_x-free hydrogen producing technologies are developed. Step-wise reforming of hydrocarbons appears to be a promising route for production of clean hydrogen. Although a large number of studies have been undertaken on hydrocarbon decomposition (Step I of the process), relatively few investigations have addressed the combined process. Further in-depth studies will be

required to probe the commercial feasibility of the process for CO-free production of hydrogen for the PEM cells. Future studies should address issues such as catalyst design (effect of promoters) and stability, reactor operation (optimum reaction temperature, pressure and feed switch over times) and design (e.g. parallel fixed bed reactors, fluidized bed reactors). It is also extremely important to investigate the effect of commonly encountered poisons such as sulfur on the step-wise reforming process.

PROX represents an extremely efficient method for trace CO removal from reformate streams. Supported Pt and Au catalysts have been extensively investigated for the PROX reaction; while Au-based catalysts are more active at the desired operating conditions, the Pt catalysts are more stable. However, it is essential to minimize the use of Pt in view of its poor requirement/supply statistics. It may be worthwhile to investigate other systems such as Ru/Rh and bimetallic catalysts for the PROX reaction. Improvements in both catalyst design as well as reactor design are currently desired for PROX.

Amongst the low temperature fuel cells, AFC has a unique advantage in that it can use non-Pt electrodes. Ammonia is an excellent source of hydrogen for applications in these fuel cells systems. Although studies have shown that Ru, Ir and Ni-based catalysts are active for ammonia decomposition, further investigations (catalyst design) directed towards obtaining near equilibrium conversions need to be undertaken.

Acknowledgements

We acknowledge with pleasure the support of this work by the Department of Energy, Office of Basic Sciences, Division of Chemical Sciences.

References

[1] A.J. Appleby, F.R. Foulkes, Fuel Cell Handbook, Van Nostrand Reinhold, New York, 1989.
[2] J.R. Rostrup-Nielsen, in: J.R. Anderson, M. Boudart (Eds.), Catalytic Steam Reforming, Science and Engineering, vol. 5, Springer, Berlin, 1984.
[3] J.N. Armor, Appl. Catal. 176 (1999) 159.
[4] V.R. Choudhary, A.S. Mamman, S.D. Sansare, Angew. Chem. Int. Ed. Engl. 31 (1992) 1189.
[5] J.R. Rostrup-Nielson, Catal. Today 18 (1993) 305.
[6] J.M. Thomas, W.J. Thomas, Principles and Practice of Heterogeneous Catalysis, VCH, Weinheim, 1997.
[7] N. Vanderborgh, Private Communication, 2000.
[8] T.V. Choudhary, D.W. Goodman, Catal. Lett. 59 (1999) 93.
[9] T.V. Choudhary, D.W. Goodman, J. Catal. 192 (2000) 316.
[10] T.V. Choudhary, C. Sivadinarayana, C. Chusuei, A. Klinghoffer, D.W. Goodman, J. Catal. 199 (2001) 9.
[11] T. Zhang, M.D. Amiridis, Appl. Catal. A 167 (1998) 161.
[12] R. Metkemeijer, P. Achard, Int. J. Hydrogen Energy 19 (1994) 535.
[13] R. Metkemeijer, P. Achard, J. Power Sources 49 (1994) 271.
[14] T.V. Choudhary, C. Sivadinarayana, D.W. Goodman, Catal. Lett. 72 (2001) 197.
[15] T.V. Choudhary, A. Santra, C. Sivadinarayana, B.K. Min, C. Yi, K. Davis, D.W. Goodman, Catal. Lett. 77 (2001) 1.
[16] M. Belgued, P. Pareja, A. Amariglio, H. Amariglio, Nature 352 (1991) 789.
[17] T. Koerts, M.J. Deelen, R.A. Van Santen, J. Catal. 138 (1992) 101.
[18] M.M. Koranne, G.W. Zajac, D.W. Goodman, Catal. Lett. 30 (1995) 219.
[19] P.L. Solomun, M.-C. Wu, D.W. Goodman, Catal. Lett. 25 (1994) 75.
[20] T.P. Beebe Jr., D.W. Goodman, J.T. Yates Jr., J. Chem. Phys. 87 (1987) 2305;
M.-C. Wu, D.W. Goodman, Catal. Lett. 24 (1994) 23;
M.-C. Wu, D.W. Goodman, Surf. Sci. Lett. 306 (1994) L529;
M.-C. Wu, Q. Xu, D.W. Goodman, J. Phys. Chem. 98 (1994) 5104.
[21] Y.-N. Wang, R.G. Herman, K. Klier, Surf. Sci. 279 (1992) 33.
[22] T.V. Choudhary, D.W. Goodman, J. Mol. Catal. 163 (2000) 9.
[23] M. Steinberg, Energy Conv. Mgmt. 36 (1995) 791.
[24] N.Z. Muradov, Energy Fuels 12 (1998) 41.
[25] P. Ferreira-Aparicio, I. Rodriguez-Ramos, A. Guerrero-Ruiz, Appl. Catal. A 148 (1997) 343.
[26] T.V. Choudhary, C. Sivadinarayana, A. Klingerhoffer, D.W. Goodman, Stud. Surf. Sci. Catal. 136 (2001) 197.
[27] S.K. Shaikhutdinov, V.I. Zaikovskii, L.B. Avdeeva, Appl. Catal. A. 148 (1996) 123.
[28] M.A. Ermakova, D.Y. Ermakov, G.G. Kuvshinov, L.M. Plyasova, J. Catal. 187 (1999) 77.
[29] R.T.K. Baker, Carbon 27 (1989) 315.
[30] R.T.K. Baker, J.J. Chludzinski Jr., J. Catal. 64 (1980) 464.
[31] M.S. Kim, N.M. Rodriguez, R.T.K. Baker, J. Catal. 134 (1992) 253.
[32] N.M. Rodriguez, J. Mater. Res. 8 (1993) 3233.
[33] Y.D. Li, J.L. Chen, Y.N. Qin, L. Chang, Energy Fuels 14 (2000) 1188.
[34] G.G. Kushinov, Y.I. Mogilnykh, D.G. Kushinov, V.I. Zaikovskii, L.B. Avdeeva, Carbon 36 (1998) 87.
[35] Y.D. Li, J.L. Chen, L. Chang, Y.N. Qin, J. Catal. 178 (1998) 76.
[36] P. Chen, X. Wu, J. Lin, K.L. Tan, Science 285 (1999) 91.
[37] N.M. Rodriguez, M.S. Kim, R.T.K. Baker, J. Phys. Chem. 98 (1994) 13108.

[38] K.P. De Jong, J.W. Gues, Catal. Rev.-Sci. Eng. 42 (2000) 481.
[39] S.K. Shaikhutdinov, L.B. Avdeeva, B.N. Novgorodov, V.I. Zaikovskii, D.I. Kochubey, Catal. Lett. 47 (1997) 35.
[40] K. Otsuka, S. Kobayashi, S. Takenaka, Appl. Catal. A 190 (2000) 261.
[41] K. Otsuka, S. Kobayashi, S. Takenaka, Appl. Catal. A 210 (2001) 371.
[42] A. Steinfield, V.A. Kirillov, G.G. Kushinov, Y.I. Mogilnykh, A. Reller, Chem. Eng. Sci. 52 (1997) 3599.
[43] A. Meier, V.A. Kirillov, G.G. Kushinov, Y.I. Mogilnykh, A. Weidenkaff, A. Steinfield, J. Phys. IV 9 (1999) 393.
[44] E. Kikuchi, Cattech 1 (1997) 67.
[45] T. Ishihara, Y. Miyashita, H. Iseda, Y. Takita, Chem. Lett. (1995) 93.
[46] K. Murata, T. Hayakawa, K. Suzuki, S. Hamakawa, Sekiyu Gakkaishi, J. Jap. Petr. Inst. 43 (2000) 162.
[47] K. Cox, K. Williamson, Hydrogen: Its Technology and Implications, vol 1, CRC Press, Boca Raton, FL, 1977.
[48] C. Sivadinarayana, T.V. Choudhary, L. Daemon, J. Eckert, D.W. Goodman, Angew. Chem. Int. Ed. 41 (2002) 144.
[49] R. Aiello, J.E. Fiscus, H.-C.Z. Loye, M.D. Amiridis, Appl. Catal. A Gen. 192 (2000) 227.
[50] V.R. Choudhary, S. Banerjee, A.M. Rajput, J. Catal. 198 (2001) 136.
[51] B. Monnerat, L. Kiwi-Minsker, A. Renken, Chem. Eng. Sci. 56 (2001) 633.
[52] C. Marquez-Alvarez, E. Odier, L. Pinaeva, Y. Schuurman, C. Millet, C. Mirodatos, Stud. Surf. Sci. Catal. 136 (2001) 483.
[53] K. Otsuka, A. Mito, S. Takenaka, I. Yamanaka, Int. J. Hydrogen Energy 26 (2001) 91.
[54] K. Otsuka, A. Mito, S. Takenaka, I. Yamanaka, Stud. Surf. Sci. Catal. 136 (2001) 215.
[55] K. Otsuka, T. Seino, S. Kobayashi, S. Takenaka, Chem. Lett. (1999) 1179.
[56] J.G.E. Cohn, US Patent No. 3,216,783 (1965).
[57] J.C. Bonacci, US Patent No. 4,238,468 (1980).
[58] N.E. Vanderborgh, C.A. Spirio, J.R. Huff, Extended Abstract of the International Seminar on Fuel Cell Technology and Applications, Hague, Netherlands, 1987, p. 253.
[59] Se H. Oh, R.M. Sinkevitch, J. Catal. 142 (1993) 254.
[60] M.J. Kahlich, H.A. Gasteiger, R.J. Behm, J. Catal. 171 (1997) 93.
[61] M.M. Schubert, H.A. Gasteiger, R.J. Behm, J. Catal. 172 (1997) 256.
[62] M. Watanabe, H. Uchida, H. Igarashi, M. Suzuki, Chem. Lett. (1995) 21.
[63] H. Igarashi, H. Uchida, M. Suzuki, Y. Sasaki, M. Watanabe, Appl. Catal. A 159 (1997) 159.
[64] M. Haruta, S. Tsubota, T. Kobayashi, H. Kageyama, M.J. Genet, B. Delmon, J. Catal. 144 (1993) 175.
[65] M. Okamura, S. Nakamura, S. Tsubota, T. Nakamura, M. Azuma, M. Haruta, Catal. Lett. 51 (1998) 53.
[66] M. Valden, X. Lai, D.W. Goodman, Science 281 (1998) 1647.
[67] M. Okumura, K. Tanaka, A. Ueda, M. Haruta, Solid State Ionics 95 (1997) 143.
[68] M. Haruta, N. Yamada, T. Kobayashi, S. Iijima, J. Catal. 115 (1989) 301.
[69] Y. Yuan, A.P. Kozlova, K. Akasura, H. Wan, K. Tsai, Y. Iwasawa, J. Catal. 170 (1997) 191.
[70] M.A. Bollinger, M.A. Vannice, Appl. Catal. B 8 (1996) 417.
[71] K. Ruth, M. Hayes, R. Burch, S. Tsubota, M. Haruta, Appl. Catal. B Environ. 24 (2000) L133.
[72] R.M.T. Sanchez, A. Ueda, K. Tanaka, M. Haruta, J. Catal. 168 (1997) 125.
[73] G.K. Bethke, H.H. Kung, 194 (2000) 43.
[74] R.J.H. Griesel, B.E. Nieuwenhuys, J. Catal. 199 (2001) 48.
[75] M.J. Kahlich, H.A. Gasteiger, R.J. Behm, J. Catal. 182 (1999) 430.
[76] M. Valden, S. Pak, X. Lai, D.W. Goodman, Catal. Lett. 56 (1998) 7.
[77] G.C. Bond, D.T. Thompson, Catal. Rev.-Sci. Eng. 41 (1999) 319.
[78] T.V. Choudhary, D.W. Goodman, Top. Catal. 21 (2002) 25.
[79] X.F. Lai, D.W. Goodman, J. Mol. Catal. A 162 (2000) 33.
[80] A. Kolmakov, D.W. Goodman, Catal. Lett. 70 (2000) 93.
[81] A. Kolmakov, D.W. Goodman, Surf. Sci. Lett. 490 (2001) L597.
[82] T.V. Choudhary, C. Sivadinarayana, C. Chusuei, A.K. Datye, J.P. Fackler Jr, D.W. Goodman, J. Catal. 207 (2002) 247.
[83] Y. Teng, H. Sakurai, A. Ueda, T. Kobayashi, Int. J. Hydrogen Energy 24 (1999) 355.
[84] M.M. Schubert, M.J. Kahlich, G. Feldmeyer, M. Huttner, S. Hackenberg, H.A. Gasteiger, R.J. Behm, Phys. Chem. Chem. Phys. 3 (2001) 1123.
[85] G. Ertl, M. Huber, J. Catal. 61 (1980) 537.
[86] E. Shustorovich, A.T. Bell, Surf. Sci. Lett. 259 (1991) L791–L796.
[87] D.G. Loffler, L.D. Schmidt, J. Catal. 44 (1976) 244.
[88] A.P.C. Reed, R.M. Lambert, J. Phys. Chem. 88 (1984) 1954.
[89] D. Chryssostomou, J. Flowers, F. Zaera, Surf. Sci. 439 (1999) 34.
[90] M. Grossman, D.G. Loffler, J. Catal. 80 (1983) 188.
[91] G. Papapolymerou, V. Bontozoglou, J. Mol. Catal. 120 (1997) 165.
[92] M. Grosman, D.G. Loffler, React. Kinet. Catal. Lett. 33 (1987) 87.
[93] R.W. McCabe, 79 (1983) 445.
[94] A.K. Santra, B.K. Min, C.W. Yi, K. Luo, T.V. Choudhary, D.W. Goodman, J. Phys. Chem. B 106 (2002) 340.
[95] S.R. Logan, C. Kemball, Trans. Faraday Soc. 56 (1960) 144.
[96] W. Tsai, W.H. Weinberg, J. Phys. Chem. 91 (1987) 5307.
[97] M.C.J. Bradford, P.E. Fanning, M.A. Vannice, J. Catal. 172 (1997) 479.
[98] K. Hashimoto, N. Toukai, J. Mol. Catal. 161 (2000) 171.
[99] Z. Kowalczyk, J. Sentek, S. Jodzis, M. Muller, O. Hinrichsen, J. Catal. 169 (1997) 407.
[100] W. Rarog, Z. Kowalczyk, J. Sentek, D. Skladanowski, D. Szmigiel, J. Zielinski, Appl. Catal. A 208 (2001) 213.